Tissue Engineering

Tissue Engineering Manuscript Central: http://mc.manuscriptcentral.com/ten

MODULATING THE PHYSICAL MICROENVIRONMENT TO STUDY REGENERATIVE PROCESSES IN VITRO USING CELLS FROM MOUSE PHALANGEAL ELEMENTS

Journal:	*Tissue Engineering*
Manuscript ID:	TEA-2012-0503.R1
Manuscript Type:	Original Article
Date Submitted by the Author:	n/a
Complete List of Authors:	Lynch, Kristen; Tulane University, Biomedical Engineering Ahsan, Tabassum; Tulane University, Biomedical Engineering
Keyword:	Tissue Development and Growth < Fundamentals of Tissue Engineering, Composite Tissue < Tissue Engineering Applications, 3-D Cell Culture < Enabling Technologies, Wound Healing < Fundamentals of Tissue Engineering, Cell Migration < Fundamentals of Tissue Engineering
Abstract:	Epimorphic regeneration in humans of complex multi-tissue structures is primarily limited to the digit tip. In a comparable mouse model, the response is level-specific in that regeneration occurs after amputation at the distal end of the terminal phalanx, but not more proximally. Recent isolation of stromal cells from CD1 murine phalangeal elements two and three (P2 and P3) allow for comparative studies of cells prevalent at the amputation plane of a more proximal region (considered non-regenerative) and a more distal region (considered regenerative), respectively. This study used adherent, suspension, and collagen gel cultures to investigate cellular processes relevant to the initial response to injury. Overall, P2 cells were both more migratory and able to compact collagen gels to a greater extent compared to P3 cells. This observed increased capacity of P2 cells to generate traction forces was likely related to the higher expression of key cytoskeletal proteins (e.g. microfilament, non-keratin intermediate filaments, and microtubules) compared to P3 cells. In contrast, P3 cells were found to be more proliferative than P2 cells under all three culture conditions and to have higher expression of keratin proteins. In addition, when cultured in suspension rather than on adherent surfaces, P3 cells were both more proliferative and had greater gene expression for matrix proteins. Together these results add to the known inherent differences in these stromal cells by characterizing responses to the physical microenvironment. Furthermore, while compaction by P2 cells confirm that collagen gels is a useful model to study wound healing, the response of P3 cells indicate that suspension culture, in which cell-cell interactions dominate like in the blastema, may be better suited to study regeneration. Therefore, this study can help develop clinical strategies for promoting regeneration through increased understanding in the properties of cells involved in endogenous repair as well as informed selection of useful in vitro models.

MODULATING THE PHYSICAL MICROENVIRONMENT TO STUDY REGENERATIVE PROCESSES *IN VITRO* USING CELLS FROM MOUSE PHALANGEAL ELEMENTS

Kristen M. Lynch & Taby Ahsan, Ph.D.*

Department of Biomedical Engineering
Tulane University
500 Lindy Boggs Center
New Orleans, LA 70118

Running Title: Physical Microenvironment & Regeneration

Kristen M. Lynch
Tulane University
Department of Biomedical Engineering
500 Lindy Boggs Center
New Orleans, LA USA 70118
PHONE: (504) 865-5178
FAX: (504) 862-8779
EMAIL: klynch2@tulane.edu

*Corresponding author
Taby Ahsan
Tulane University
Department of Biomedical Engineering
500 Lindy Boggs Center
New Orleans, LA USA 70118
PHONE: (504) 865-5899
FAX: (504) 862-8779
EMAIL: tahsan@tulane.edu

Date: August 19, 2012

Mary Ann Liebert, Inc.,140 Huguenot Street, New Rochelle, NY 10801

ABSTRACT

Epimorphic regeneration in humans of complex multi-tissue structures is primarily limited to the digit tip. In a comparable mouse model, the response is level-specific in that regeneration occurs after amputation at the distal end of the terminal phalanx, but not more proximally. Recent isolation of stromal cells from CD1 murine phalangeal elements two and three (P2 and P3) allow for comparative studies of cells prevalent at the amputation plane of a more proximal region (considered non-regenerative) and a more distal region (considered regenerative), respectively. This study used adherent, suspension, and collagen gel cultures to investigate cellular processes relevant to the initial response to injury. Overall, P2 cells were both more migratory and able to compact collagen gels to a greater extent compared to P3 cells. This observed increased capacity of P2 cells to generate traction forces was likely related to the higher expression of key cytoskeletal proteins (e.g. microfilament, non-keratin intermediate filaments, and microtubules) compared to P3 cells. In contrast, P3 cells were found to be more proliferative than P2 cells under all three culture conditions and to have higher expression of keratin proteins. In addition, when cultured in suspension rather than on adherent surfaces, P3 cells were both more proliferative and had greater gene expression for matrix proteins. Together these results add to the known inherent differences in these stromal cells by characterizing responses to the physical microenvironment. Furthermore, while compaction by P2 cells confirm that collagen gels is a useful model to study wound healing, the response of P3 cells indicate that suspension culture, in which cell-cell interactions dominate like in the blastema, may be better suited to study regeneration. Therefore, this study can help develop clinical strategies for promoting regeneration through increased understanding in the properties of cells involved in endogenous repair as well as informed selection of useful *in vitro* models.

Mary Ann Liebert, Inc.,140 Huguenot Street, New Rochelle, NY 10801

INTRODUCTION

Species such as salamanders and newts can undergo epimorphic regeneration, which includes the replacement of whole limbs (1). In mice (2-4) and humans (5, 6), however, regeneration of complex multi-tissue structures is primarily limited to regeneration of the distal digit tip. Animal models have been pivotal in determining key signaling pathways (7, 8) and cell sources (9, 10) involved in regeneration. In addition, recent tissue engineering studies have begun to test treatment modalities to help promote whole digit and limb regeneration (11, 12). Use of *in vitro* techniques with mammalian cells, however, is also essential to increase understanding of the cellular processes involved in injury responses to amputation.

It is unclear the relative contribution of the different endogenous cells to the regenerative process. It was originally thought that the blastema was a homogenous population of dedifferentiated cells that form the base of tissue regrowth (13). More recent studies have found that multiple lineage-restricted tissue stem/progenitor cells contribute to the blastema in the urodele limb and mouse digit tip (9, 10, 14). Regardless of cell source, complete repair of the digit tip ultimately involves multiple specialized phenotypes including endothelial cells, mesenchymal stem cells, fibroblasts, and skeletal cells.

Comparison of the native cells from regenerating and non-regenerating regions of the digit can be useful to help identify cellular attributes necessary for the restoration of lost tissue. Regenerative processes in mammalian digit tips is level-specific in that amputation at the distal end leads to regeneration while a more proximal injury leads to wound healing (3). These outcome differences occur despite fairly similar cellular and tissue components at the original site of injury. Recent isolation of skeletal cells from mouse phalangeal element three (regenerating region; P3) and phalangeal element two (non-regenerating region; P2) (15) allow

Mary Ann Liebert, Inc.,140 Huguenot Street, New Rochelle, NY 10801

for studies with a major phenotype prevalent at the amputation plane. Comparative *in vitro* studies using these cells will improve understanding of the processes that limit or drive regeneration.

Complex aspects of the *in vivo* microenvironment are known to mediate cell processes. Use of adherent, suspension and scaffold-based cultures *in vitro* can help establish the effects of physical configuration on cell proliferation, migration, and function. The objective of these early studies with P2 and P3 cells was to determine phenotypic differences in response to culture environment.

MATERIALS & METHODS

Phalangeal Element (P2 and P3) Cells

Cells were previously isolated from week 8 adult CD1 mice [(15), a generous gift from Dr. Ken Muneoka of Tulane University] through digestion of the skeletal connective tissue of phalangeal elements (separated from the adjacent skin, fur, fat pad, nail and ligament tissue) of digits II-IV (15). The adherent cells from mouse phalangeal element 2 (P2: from middle phalanx) and 3 (P3: from terminal phalanx) were then expanded using Fibronectin-coated (Fn; 3.5 μg/cm^2) dishes in culture medium, which consisted of Dulbecco's Modification of Eagles Medium/MCDB supplemented with ITS+1 (Sigma), 5% ES-qualified fetal bovine serum (Invitrogen), 10^{-9} M Dexamethasone (Sigma), 10^{-4} Ascorbic Acid 2-phosphate (Sigma), 50 μg/ml PDGFββ, 50 μg/ml EGF (R &D Systems), 1000 U/ml Leukemia Inhibitory Factor (EMD Millipore) and antibiotics (16).

Culture Conditions

Cells were cultured under both two- and three- dimensional (2D and 3D, respectively) conditions. In adherent 2D culture, cells were seeded at 8,000 per cm^2 on Fn-coated tissue

Mary Ann Liebert, Inc.,140 Huguenot Street, New Rochelle, NY 10801

culture plastic (Fn-TCP). To provide a 3D culture environment, cells were either put into suspension (SUS) or collagen gels (GEL) (17). For SUS cultures, expanded cells were placed into bacteriological petri dishes (0.5 E6 cells/100 mm dish) and continuously agitated on an orbital shaker (40 RPM). Cells were maintained for up to 12 days, with culture medium and dishes changed every other day. For GEL cultures, expanded cells were encapsulated into type I collagen gels (2 mg/ml) with an initial seeding density of 0.2 E6 cells/ml. Each gel (0.75 ml) was polymerized overnight in 12-well plates and then released to allow for unconstrained compaction. GEL samples were maintained for up to 8 days with medium changed every two days (25 ml/gel).

Cell Proliferation

Cell proliferation was evaluated by quantification of number and cell cycle phase. Number was determined for cells recovered from trypsinized Fn-TCP samples and collagenase- digested (600 U/ml, type 2; Worthington Biochemical) GEL samples using the Z1 COULTER COUNTER® (counts >6 μm). Cell cycle phases were assessed by recovering single cell solutions either by trypsinization of Fn-TCP samples or dissociation of SUS samples, staining with DRAQ5 (Biostatus, Leicestershire, UK), analyzing fluorescence using a FACS Canto (BD Biosciences), and fitting for phase distribution using FCS Express Software v4.

Scratch Test

Cell migration was evaluated for confluent monolayers of P2 and P3 cells on Fn-coated glass slides. A 1000 μL pipet tip was used to create a scratch approximately 240 μm wide that was then imaged at 0, 3, and 6 hours. For better visualization of outstretched cellular processes, samples were fixed at 6 hours, stained for F-actin using Phalloidin (Invitrogen), and imaged using standard fluorescent microscopy.

Gene Expression

At the end of culture, cells from Fn-TCP samples and cell clusters from SUS samples were lysed, homogenized using Qiagen QIAshredders, and stored at -80°C until further processing. RNA was isolated from the frozen cell lysates and the GEL samples using the Qiagen RNeasy and RNeasy Lipid Tissue kits, respectively, and each sample was quantified using a Nanodrop® spectrophotometer. Standard analysis of mRNA levels for each sample was done on cDNA converted from 1 µg RNA (Invitrogen Superscript® III First-strand synthesis) and analyzed using SYBR® Green on a StepOnePlus™ PCR System (Applied Biosystems). Primers were custom designed (Primer Express® Software v3) for microfilaments (ACTA1, ACTA2), intermediate filaments (KRT6A, KRT8, KRT13, LMNA, and VIM), microtubule (TUBA1B) and ECM proteins (FN1, COL1A1, and COL4A1). (Primer sequences are listed in Supplemental Table 1.) Gene expression levels were quantified using standard curves and are all reported as normalized to GAPDH expression.

Analysis of genes associated with signal transduction pathways was performed using an RT2 Profiler™ PCR array (SA Biosciences). RNA from three independent samples per group were converted to cDNA and analyzed using the vendor's specified reagents and instructions. For each sample, 84 signal transduction genes were normalized to housekeeping genes. Fold regulation between groups was used to evaluate differences in expression due to either cell type or culture condition. (Complete listing of genes, fold regulation, and p-values are found in Supplemental Table 2.)

Microscopy

Images of Fn-TCP, SUS, and GEL samples were taken periodically during culture, as well as after histological processing at terminal timepoints. Phase images were taken of Fn-TCP and SUS samples, while macroscopic pictures were taken of GEL samples. To quantify

changes in cell cluster and collagen gel size over time, cross sectional areas of individual SUS and GEL samples were calculated using analysis (ImageJ software) of calibrated images. Spatial distribution of cells in 3D culture conditions was also visualized, where fixed SUS and GEL samples were paraffin processed, cut into 7 μm sections, stained with hematolylin and eosin (H & E), and imaged under brightfield conditions.

Statistical Analysis

Data are presented as mean±SEM. A student's t-test was used to compare P2 versus P3 cells, as well as FN-TCP versus SUS culture conditions. These separate comparisons between cell types or between culture conditions were considered significant with p-values of <0.05.

RESULTS

Culture on Tissue Culture Plastic (FN-TCP)

P2 and P3 cells attached and proliferated on Fn-TCP, although images of P3 cultures showed a greater presence of light-refractive edges (Fig. 1A, B). Quantification of cell number after two and a half days resulted in a 5.7- and 8.6- fold increase over the initial seeding density for P2 and P3 cells, respectively (Fig. 1C). The P3 value, however, was 50% higher ($p<0.05$), indicating a greater proliferative rate for P3 cells. Cell cycle analysis was consistent with this finding, in that the fitted percentage for the DNA replicating S-phase was approximately 2-fold higher for P3 cells (31% for P2 vs 56% for P3 in Fig. 1D and E, respectively). These observed differences in proliferation between P2 and P3 cells may be due to cell cycle inhibitors, as both CDKN2A and CDKN2B were found to be upregulated (each >300X with $p<0.001$) in P2 cells using PCR arrays (Fig. 2A).

Mary Ann Liebert, Inc.,140 Huguenot Street, New Rochelle, NY 10801

Response of P2 and P3 cells to a generated scratch indicated differences in migratory potential. The initial scratch was similar in size (240 μm) for samples of both groups (Fig. 3A, D). Within 3 hours, P2 cells had begun to span the distance with a small number of cells from opposing sides in direct contact (Fig. 3B). Larger sections of the edges came into contact by 6 hours (Fig. 3C), with staining for F-actin highlighting individual P2 cells reaching across the gap (Fig. 3G). In contrast, for P3 cultures the gap between the edges of the original scratch narrowed (Fig. 3D-F), but the margins remained largely defined (Fig. 3F) with few cells reaching across (Fig. 3H). These results therefore indicate that P2 cells may have an increased migratory capacity compared to P3 cells.

Cytoskeletal gene expression is markedly different for P2 and P3 cells on Fn-TCP. To span the variety of cytoskeletal proteins that are present in cells, we assessed genes for microtubules, intermediate filaments, and microfilaments. P2 cultures had a 1.5-fold increase for TUBA1B (Fig. 4A), a 2-fold increase for both LMNA and VIM (Fig. 4B), and a 4-fold increase for ACTA-1 and -2 (Fig. 4C). Keratin intermediate filaments, however, were more highly expressed in P3 samples with a 4-fold increase for both KRT6A and KRT13 and an increase of more than an order of magnitude for KRT8 (Fig. 4D). Thus, P3 cells are more proliferative while P2 cells are more migratory on adherent culture, possibly due to cytoskeletal differences.

Culture in Suspension (SUS)

Single cell solutions of P3 cells placed into continuously agitated suspension culture form cell clusters that increased in size with time. P3 cells through aggregation and/or proliferation formed clusters comprised of multiple cells within 4 days (Fig. 5D). At Day 8, clusters were still loosely connected and transparent (Fig. 5E), though most seemed tightly-packed with dense central regions by Day 12 (Fig. 5F). Overall cluster size also changed with

Mary Ann Liebert, Inc.,140 Huguenot Street, New Rochelle, NY 10801

time (Fig. 5J-L), with the average cross-sectional area increasing from 2350 μm^2 at Day 4 to 7720 μm^2 at Day 12.

Histological sections of P3 SUS samples indicated granular matrix between individual cells within the clusters (Fig. 6A, arrow). Quantification of mRNA did show a significant ($p<0.01$) upregulation of gene expression of the ECM proteins collagen type I, collagen type IV, and fibronectin for P3 cells in SUS compared to Fn-TCP (Fig. 6B-D). Furthermore, overall greater matrix dynamics for SUS cultures was also due to a notable increase compared to Fn-TCP controls (>1500X; $p<0.001$) for matrix metalloprotease 10 (MMP10; Fig. 2B, Supplemental Table 2). Therefore in suspension, P3 cells seem to aggregate and proliferate, with the capacity to synthesize and remodel secreted matrix proteins.

P2 cells may have a preference for culture on adherent surfaces rather than in suspension. As early as Day 4, differences between cell types were detected where P2 clusters in SUS were markedly fewer (Fig. 5A) and averaged only 820 μm^2 in size (33% of time matched P3 samples). From Day 4 to Day 8, P2 clusters increased in size but remained smaller than in comparable P3 samples (Fig. 5B, J, K). The persisting P2 clusters at Day 12, however, were similar in size to those in P3 samples (Fig. 5L) but extremely few in number (Fig. 5C). This lack of P2 cells in SUS may be partly due to the negligible percentage of proliferating cells (<1% in the S-phase at Day 4; Fig. 5G), unlike P3 cells which maintained proliferative rates similar to that in Fn-TCP (59%; Fig. 5H). Furthermore, P2 cells were observed attached to the non TC-treated surfaces despite frequent petri dish changes (Fig. 5I), indicating an aversion to suspension conditions.

Culture in Type I Collagen Gels (GEL)

Encapsulation in collagen gels was found to support the *in vitro* culture of both P2 and P3 cells. Proliferation rates were quite low for both cell types, as there were less than two

Mary Ann Liebert, Inc.,140 Huguenot Street, New Rochelle, NY 10801

population doublings over four days (Fig. 7A), though P3 cell number was slightly higher ($p<0.05$). Histological sections revealed that cells were still homogenously and sparsely distributed after 4 days with an initial seeding density of 1.5 E5 cells per 0.75 ml GEL. By Day 8, however, P2 samples had an accumulation of cells at the free GEL boundary (Fig. 7, arrows) that was absent in P3 samples. This observed accumulation, despite a low proliferation rate in P2 GEL samples, and the previous results of the scratch test in adherent culture, may be due to a more migratory nature of P2 cells compared to P3 cells.

P2 and P3 cells are able to respond to the matrix environment in GEL culture. Qualitative images show that over eight days the gels compacted (Fig. 8A), which is known to be due to active cellular processes including force generation (18). Quantification of the cross-sectional area of multiple independent samples over time (Fig. 8B) revealed that P2 cells compacted the GEL not only more quickly (by 66% vs. 22% at Day 4) but also to greater levels (by 84% vs. 67% at Day 8). Considering the role of the cytoskeleton with force generation, it was not unexpected that P2 cells had significantly higher gene expression levels of microtubules, non-keratin intermediate filaments and microfilaments (Fig. 8D). As was found on Fn-TCP, P3 cells did have higher levels of keratin expression (Fig. 8C), however, these proteins are not usually implicated in traction force. In addition, P2 cells had >4-fold expression levels ($p<0.05$ for each) compared to P3 cells of extracellular matrix proteins collagen type I, collagen type IV, and fibronectin (Fig. 9). Thus, in an exogenously matrix-rich environment, such as collagen type I gels, P2 cells compared to P3 cells have a greater ability to remodel the surrounding microenvironment.

Mary Ann Liebert, Inc.,140 Huguenot Street, New Rochelle, NY 10801

DISCUSSION

These *in vitro* studies explored cellular processes of P2 and P3 cells in 2D and 3D culture. P3 cells were found to be more proliferative when compared to P2 cells for adherent, suspension, and collagen gel cultures. Moreover, P2 cells were almost completely non-proliferative when presented with no exogenous matrix proteins, as in suspension culture. Cell mobility, conversely, was primarily observed in P2 samples which were able to span gaps on 2D glass slides and accumulate at the free edges of 3D gels. In addition, P2 cells contracted collagen gels to a greater degree than P3 cells. These observed changes in cell functionality may be partly due to the stark differences in expression of cytoskeletal proteins, which were all greater in P2 cells except for the keratins.

The use of cells isolated from mouse phalangeal elements two and three, which are considered regions of non-regenerative and regenerative potential, respectively, allow for *in vitro* comparative studies using mammalian cells. Here we used simple culture paradigms that controlled the microenvironmental cues and focused on a single phenotype, skeletal cells. There is the possibility of population heterogeneity, as evidenced by a small distinct subpopulation in the P2-SUS cultures at later timepoints. These studies, however, were still able to identify discernible population differences based on original tissue location in terms of proliferation, migration, force generation, and cytoskeleton expression. The higher expression of keratin proteins in the P3 cells compared to the P2 cells, expected due to the close proximity and potential regenerative involvement of the nail bed at the terminal phalanx (19), substantiate that the differences observed in these *in vitro* cultures are likely reflective of inherent *in situ* cell differences. Ultimate regeneration with tissue outgrowth *in vivo*, however, not only depends on factors intrinsic to the cells, but also extrinsic cues (20). Thus, subsequent *in vitro* studies need to provide a more complex microenvironment, allowing spatiotemporal

Mary Ann Liebert, Inc.,140 Huguenot Street, New Rochelle, NY 10801

regulation of cytokines, heterotypic cell-cell interactions, and cell-matrix binding, to properly investigate the different phases of regeneration.

Wound healing and regeneration have distinct goals, i.e. survival versus restoration of function, that lead to different tissue outcomes. Wound healing commences with an inflammatory response, followed by re-epithelization and matrix synthesis, and is completed by matrix remodeling (21). Regeneration in the mouse digit tip undergoes similar initial processes, but then progresses to blastema formation, and tissue outgrowth (22). Though regeneration ultimately forms complex multi-tissue structures, it has been suggested that differences in the early cellular responses (13), including proliferation, migration, and contraction, may prescribe the end result (23). Thus, the model systems used here were selected to investigate events relevant to the initial response after amputation.

Cell proliferation is a necessary component not only for tissue outgrowth, but also for blastema formation. Cells in the blastema are not just those resident at the time of injury but also their progeny, with certain phenotypes over-represented compared to original availability (9, 10, 24). In our studies, we found that cells from the regenerative P3 element had markedly higher proliferative rates *in vitro* compared to similar cells from the non-regenerative P2 element, with the greatest differences seen in suspension cultures. Such differences may be due to regulation of cell cycle inhibitors, which were more highly expressed for P2 cells. In conjunction with the propensity of P2 cells to migrate when presented with proteins (either as a basement layer in 2D or a collagenous tissue in 3D), the inability to initially amass skeletal cells as part of a stable blastema cell cluster may be one hurdle for regeneration.

The standard *in vitro* wound healing models have not been optimized to study regeneration. Contraction of granulation tissue is a key event during wound healing (25) and is mimicked in collagen gels where stromal cells induce observable levels of compaction (26).

Mary Ann Liebert, Inc.,140 Huguenot Street, New Rochelle, NY 10801

Consistent with the notion that P2 cells participate in wound healing as opposed to regeneration, it was found that P2 cells in gels were able to migrate and induce compaction to a greater extent than P3 cells. Furthermore, the markedly lower levels of ECM expression in P3-GEL samples suggest that collagen gels may not be suitable to study cells associated with regeneration. Instead suspension culture, in which cell-cell interactions dominate over cell-matrix interactions (27, 28), seems to be a more appropriate *in vitro* model to study early blastema events. As would be expected from cells native to a regenerative region, P3 cells proliferated and expressed high levels of ECM-relevant proteins when cultured in suspension. Thus, while collagen gels are frequently used to study wound healing (29), suspension cultures may be a useful model to study regenerative processes.

One of the more notable distinctions between P2 and P3 cells was cytoskeletal gene expression. As the cytoskeleton is associated with force generation (30), the higher levels of microfilament and microtubule expression in P2 cells are consistent with observations of greater migration and gel compaction. In contrast, the higher levels of keratin expression in P3 cells may not only be due to the proximity of the source tissue to the nail bed, but may be associated with the recent implication of keratins in stem cell self-renewal (10). Thus, the cytoskeleton may play a major role in the early cellular responses to injury, including proliferation, migration, and wound closure. Collectively, these studies suggest that attempts to steer injury responses from wound healing towards regeneration may involve cytoskeletal modulation.

The default response to amputation in humans is one of survival through wound healing, including an immune response to ward off infection (31) and scar tissue formation to seal the *injury* (32). The evolved efficacy of this response may in fact hinder the more sophisticated process of regeneration (32, 33). While documented cases of regeneration at the

Mary Ann Liebert, Inc.,140 Huguenot Street, New Rochelle, NY 10801

distal digit tip (5, 6) signals potential for promoting a robust regenerative response in humans, there is yet no obvious biological approach to leverage during treatment. For example, it is unclear whether to focus on redevelopment; endogenous repair of the mouse digit tip relies on secondarily evolved processes (3), but exogenously-promoted repair recapitulates developmental pathways (7). In addition, the importance of blastema formation in mammalian regeneration has yet to be established, as recent studies indicate that multiple fate-restricted tissue stem cells contribute to tissue restoration (9, 10). Furthermore, while the P2 and P3 phenotypes are sourced from regions with inherently different regenerative potentials, it cannot be currently excluded that primary causal differences may be due to other factors, such as proximity to the nail bed or different scarring responses. Yet comparative studies such as ours help advance the biological understanding of endogenous cell sources that will translate into treatment modalities for digit and limb amputation.

In conclusion, our studies elucidated the distinct responses of P2 and P3 cells to different culture environments, implicated the cytoskeleton in these responses, and evaluated the relative value of each culture model for the study of regenerative processes. Specifically, we found that P3 cells were overall more proliferative while P2 cells were more migratory. In addition, P2 cells had higher expression of microfilaments, microtubules, and intermediate filaments, with the clear exception of the keratin proteins that were more highly expressed in P3 cells. Finally, we propose that suspension culture may be a better in *vitro* system to study regenerative processes than collagen gel culture, which is classically used for wound healing studies. While these types of studies lack the complete spectrum of environmental cues present during *in vivo* regeneration, the limited-factor approach of *in vitro* studies allows for confirmation of mechanisms thought to be critical *in vivo*, as well as exploration into new mechanisms and metrics of regeneration.

Mary Ann Liebert, Inc.,140 Huguenot Street, New Rochelle, NY 10801

Determining the keys to regeneration would radically alter medical treatment, yet is still among the greatest biological challenges. Study in non-mammalian species, such as salamanders and frogs, and the few available mammalian models have provided insight into some of the pathways that govern regeneration. It is not possible, however, to perform controlled mechanistic studies during the complicated regenerative process *in vivo*. Thus, the use of *in vitro* models that can spatially and temporally control environmental factors will be critical to help translate basic science studies into therapies for regeneration.

ACKNOWLEDGMENTS

The authors thank Tulane University, the Louisiana Board of Regents (KML), and the NIH (#P20 GM103629) for supporting this work. In addition, we thank Dr. Ken Muneoka, Jaime Castillo, and members of the Muneoka laboratory at Tulane University for the generous gift of the P2 and P3 cells.

AUTHOR DISCLOSURE STATEMENT

No competing financial interests exist.

Mary Ann Liebert, Inc.,140 Huguenot Street, New Rochelle, NY 10801

FIGURE LEGENDS

Figure 1. Morphology and proliferation on Fn-TCP. Phase images at lower (**LEFT**) and higher (**RIGHT**) magnification of P2 (**A**) and P3 (**B**) cells grown on Fn-coated tissue culture plastic. (**C**) Cell number for P2 and P3 cultures were counted after 2.5 days, with the dotted line representing the initial cell number (mean±SEM, n=5, *for $p<0.05$). Histograms show fluorescence due to DRAQ5 staining for P2 (**D**) and P3 (**E**) cultures, with fitted curves for cell cycle analysis overlaid to determine percentages in the G0/G1, S, and G2 phases (indicated by separate colors).

Figure 2. Gene expression of signaling pathways. Relative expression of 84 signaling-related genes is displayed on scatter plots of P2 Fn-TCP vs P3 Fn-TCP (**LEFT**) and P3 SUS vs P3 Fn-TCP (**RIGHT**). Genes with changes ≤2-fold are indicated in black (and lie within the region marked by the lines). Changes in expression levels ≥2-fold are indicated in red (upregulation) or green (downregulation). Relative expression of CDKN2A and CDKN2B (single arrowheads), as well as MMP10 (double arrowheads) are shown.

Figure 3. Scratch test on Fn-coated glass slides. Lower (**LEFT**) and higher (**RIGHT**) magnification phase images were taken of P2 (**A-C, G**) and P3 (**D-F, H**) cultures immediately (**A, D**), 3 hr (**B, E**), and 6 hr (**C, F, G, H**) after creating a scratch of confluent monolayers. Samples fixed at 6 hr and stained with phalloidin were imaged fluorescently to visualize outstretched cellular processes.

Mary Ann Liebert, Inc.,140 Huguenot Street, New Rochelle, NY 10801

Figure 4. Cytoskeletal gene expression on Fn-TCP. P2 and P3 cultures were analyzed for microtubules (**A**: TUBA1B), intermediate filaments (**B**: LMNA, VIM; **D**: KRT6A, KRT8, KRT13), and microfilaments (**C**: ACTA1, ACTA2). Values presented are mean±SEM (n=5), with asterisks indicating p-values (* for $p<0.05$, ** for $p<0.01$).

Figure 5. Morphology and proliferation in SUS. Lower (**LEFT**) and higher (**RIGHT**) magnification phase images were taken of P2 (**A-C**) and P3 (**D-F**) cell clusters after 4 (**A, D**), 8 (**B, E**), and 12 (**C, F**) days. Histograms show fluorescence due to DRAQ5 staining for P2 (**G**) and P3 (**H**) SUS samples, with fitted curves for cell cycle overlaid to determine percentages in the G0/G1, S, and G2 phases (indicated by separate colors). (**I**) Phase image of P2 cells attached to petri dishes at Day 5. Histograms of size analysis for P2 (**BLUE**) and P3 (**RED**) cell clusters after 4 (**J**), 8 (**K**), and 12 (**L**) days.

Figure 6. Extracellular matrix of P3 cells in SUS. (A) Phase image of a D8 P3 cell cluster, arrow indicates granular matrix between cells. Relative gene expression of collagen type I (B), collagen type IV (C), and fibronectin (D) of P3 cells at D8 grown in SUS compared to Fn-TCP. Values presented are mean±SEM (n=3-5, ** for $p<0.01$).

Figure 7. Cell number and distribution in GEL samples. (**A**) Cell number was determined for P2 and P3 GEL samples after 4 days of culture, with the dotted line representing the initial cell number (mean±SEM, n=4, *for $p<0.05$). Brightfield images of P2 (B, D) and P3 (C, E) samples at 4 (B, C) and 8 (D, E) days are shown, with arrows indicating the edge of the collagen gels in cross-section.

Mary Ann Liebert, Inc.,140 Huguenot Street, New Rochelle, NY 10801

Figure 8. Compaction and cytoskeletal expression in GEL samples. Macroscopic images are shown (**A**) for P2 (**LEFT**) and P3 (**RIGHT**) GEL samples at Days 1 and 8, with cross sectional area plotted for each day to quantitate compaction (**B;** mean±SEM, n=6-15). Cytoskeletal gene expression was analyzed in Day 8 samples for keratin filaments (**C**: KRT6A, KRT8, and KRT13), as well as other cytoskeletal proteins (**D**: TUBA1B, VIM, LMNA, ACTA1, and ACTA2). Values presented are mean±SEM (n=3), with asterisks indicating p-values (* for $p<0.05$, ** for $p<0.01$).

Figure 9. Extracellular matrix in GEL samples. P2 and P3 GEL samples at Day 8 were analyzed for relative gene expression of collagen type I, collagen type IV, and fibronectin. Values presented are mean±SEM (n=3, * for $p<0.05$).

Mary Ann Liebert, Inc.,140 Huguenot Street, New Rochelle, NY 10801

REFERENCES

1. Masaki H, Ide H. Regeneration potency of mouse limbs. Dev Growth Differ.49:89-98. 2007.
2. Borgens RB. Mice regrow the tips of their foretoes. Science.217:747-50. 1982.
3. Han M, Yang X, Lee J, Allan CH, Muneoka K. Development and regeneration of the neonatal digit tip in mice. Dev Biol.315:125-35. 2008.
4. Fernando WA, Leininger E, Simkin J, Li N, Malcom CA, Sathyamoorthi S, et al. Wound healing and blastema formation in regenerating digit tips of adult mice. Dev Biol.350:301-10. 2011.
5. Douglas BS. Conservative management of guillotine amputation of the finger in children. Aust Paediatr J.8:86-9. 1972.
6. Lee LP, Lau PY, Chan CW. A simple and efficient treatment for fingertip injuries. J Hand Surg Br.20:63-71. 1995.
7. Yu L, Han M, Yan M, Lee EC, Lee J, Muneoka K. BMP signaling induces digit regeneration in neonatal mice. Development.137:551-9. 2010.
8. Wills AA, Kidd AR, 3rd, Lepilina A, Poss KD. Fgfs control homeostatic regeneration in adult zebrafish fins. Development.135:3063-70. 2008.
9. Lehoczky JA, Robert B, Tabin CJ. Mouse digit tip regeneration is mediated by fate-restricted progenitor cells. Proc Natl Acad Sci U S A.108:20609-14. 2011.
10. Rinkevich Y, Lindau P, Ueno H, Longaker MT, Weissman IL. Germ-layer and lineage-restricted stem/progenitors regenerate the mouse digit tip. Nature.476:409-13. 2011.
11. Hechavarria D, Dewilde A, Braunhut S, Levin M, Kaplan DL. BioDome regenerative sleeve for biochemical and biophysical stimulation of tissue regeneration. Medical Engineering & Physics.32:1065-73. 2010.

Mary Ann Liebert, Inc.,140 Huguenot Street, New Rochelle, NY 10801

12. Agrawal V, Johnson SA, Reing J, Zhang L, Tottey S, Wang G, et al. Epimorphic regeneration approach to tissue replacement in adult mammals. Proc Natl Acad Sci U S A.107:3351-5. 2010.

13. Gardiner DM. Ontogenetic decline of regenerative ability and the stimulation of human regeneration. Rejuvenation Res.8:141-53. 2005.

14. Kragl M, Knapp D, Nacu E, Khattak S, Maden M, Epperlein HH, et al. Cells keep a memory of their tissue origin during axolotl limb regeneration. Nature.460:60-5. 2009.

15. Wu Y. The study of stem cell like fibroblasts in mouse digit [PhD Thesis Department of Cell and Molecular Biology, Tulane Unversity, New Orleans, 2009.

16. Jiang Y, Jahagirdar BN, Reinhardt RL, Schwartz RE, Keene CD, Ortiz-Gonzalez XR, et al. Pluripotency of mesenchymal stem cells derived from adult marrow. Nature.418:41-9. 2002.

17. Pineda E, Nerem R, Ahsan T. Differentiation patterns of pluripotent stem cells in two and three dimensional culture. submitted. 2012.

18. Fernandez P, Bausch AR. The compaction of gels by cells: a case of collective mechanical activity. Integr Biol (Camb).1:252-9. 2009.

19. Han M, Yang X, Farrington JE, Muneoka K. Digit regeneration is regulated by Msx1 and BMP4 in fetal mice. Development.130:5123-32. 2003.

20. Bryant SV, Gardiner DM, Muneoka K. Limb Development and Regeneration. American Zoologist.27:675-96. 1987.

21. Broughton G, 2nd, Janis JE, Attinger CE. The basic science of wound healing. Plast Reconstr Surg.117:12S-34S. 2006.

22. Bryant SV, Endo T, Gardiner DM. Vertebrate limb regeneration and the origin of limb stem cells. Int J Dev Biol.46:887-96. 2002.

23. Yokoyama H. Initiation of limb regeneration: the critical steps for regenerative capacity. Dev Growth Differ.50:13-22. 2008.

24. Han M, Yang X, Taylor G, Burdsal CA, Anderson RA, Muneoka K. Limb regeneration in higher vertebrates: developing a roadmap. Anat Rec B New Anat.287:14-24. 2005.

25. Tomasek JJ, Gabbiani G, Hinz B, Chaponnier C, Brown RA. Myofibroblasts and mechano-regulation of connective tissue remodelling. Nature Reviews Molecular Cell Biology.3:349-63. 2002.

26. Wallace DG, Rosenblatt J. Collagen gel systems for sustained delivery and tissue engineering. Adv Drug Deliv Rev.55:1631-49. 2003.

27. Huang H, Kamm RD, Lee RT. Cell mechanics and mechanotransduction: pathways, probes, and physiology. Am J Physiol Cell Physiol.287:C1-11. 2004.

28. Schwartz MA, DeSimone DW. Cell adhesion receptors in mechanotransduction. Curr Opin Cell Biol.20:551-6. 2008.

29. Grinnell F. Fibroblasts, myofibroblasts, and wound contraction. J Cell Biol.124:401-4. 1994.

30. Alenghat FJ, Ingber DE. Mechanotransduction: all signals point to cytoskeleton, matrix, and integrins. Sci STKE.2002:pe6. 2002.

31. Singer AJ, Clark RA. Cutaneous wound healing. N Engl J Med.341:738-46. 1999.

32. Harty M, Neff AW, King MW, Mescher AL. Regeneration or scarring: an immunologic perspective. Dev Dyn.226:268-79. 2003.

33. Gurtner GC, Werner S, Barrandon Y, Longaker MT. Wound repair and regeneration. Nature.453:314-21. 2008.

Mary Ann Liebert, Inc.,140 Huguenot Street, New Rochelle, NY 10801

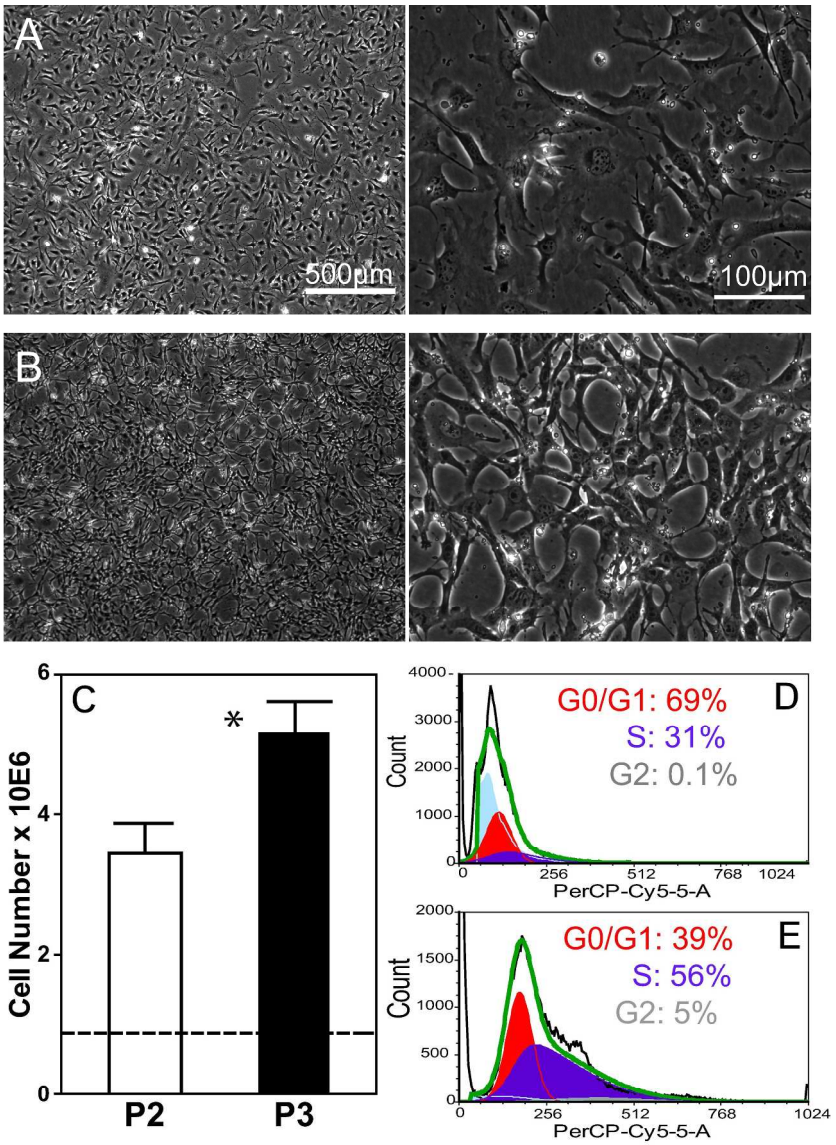

Figure 1.

Figure 1. Morphology and proliferation on Fn-TCP. Phase images at lower (LEFT) and higher (RIGHT) magnification of P2 (A) and P3 (B) cells grown on Fn-coated tissue culture plastic. (C) Cell number for P2 and P3 cultures were counted after 2.5 days, with the dotted line representing the initial cell number (mean±SEM, n=5, *for $p<0.05$). Histograms show fluorescence due to DRAQ5 staining for P2 (D) and P3 (E) cultures, with fitted curves for cell cycle analysis overlaid to determine percentages in the G0/G1, S, and G2 phases (indicated by separate colors).
215x313mm (300 x 300 DPI)

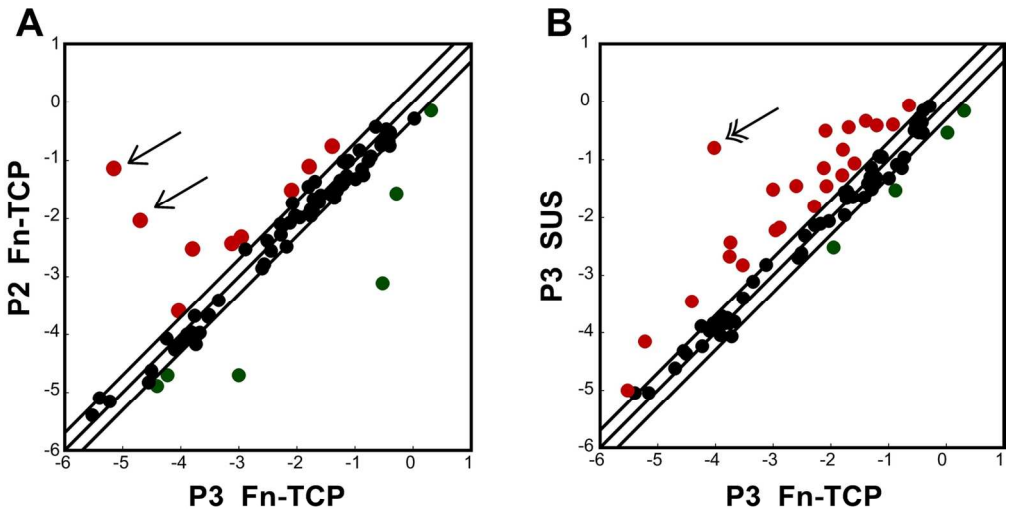

Figure 2.

Figure 2. Gene expression of signaling pathways. Relative expression of 84 signaling-related genes is displayed on scatter plots of P2 Fn-TCP vs P3 Fn-TCP (LEFT) and P3 SUS vs P3 Fn-TCP (RIGHT). Genes with changes ≤2-fold are indicated in black (and lie within the region marked by the lines). Changes in expression levels ≥2-fold are indicated in red (upregulation) or green (downregulation). Relative expression of CDKN2A and CDKN2B (single arrowheads), as well as MMP10 (double arrowheads) are shown.
142x84mm (300 x 300 DPI)

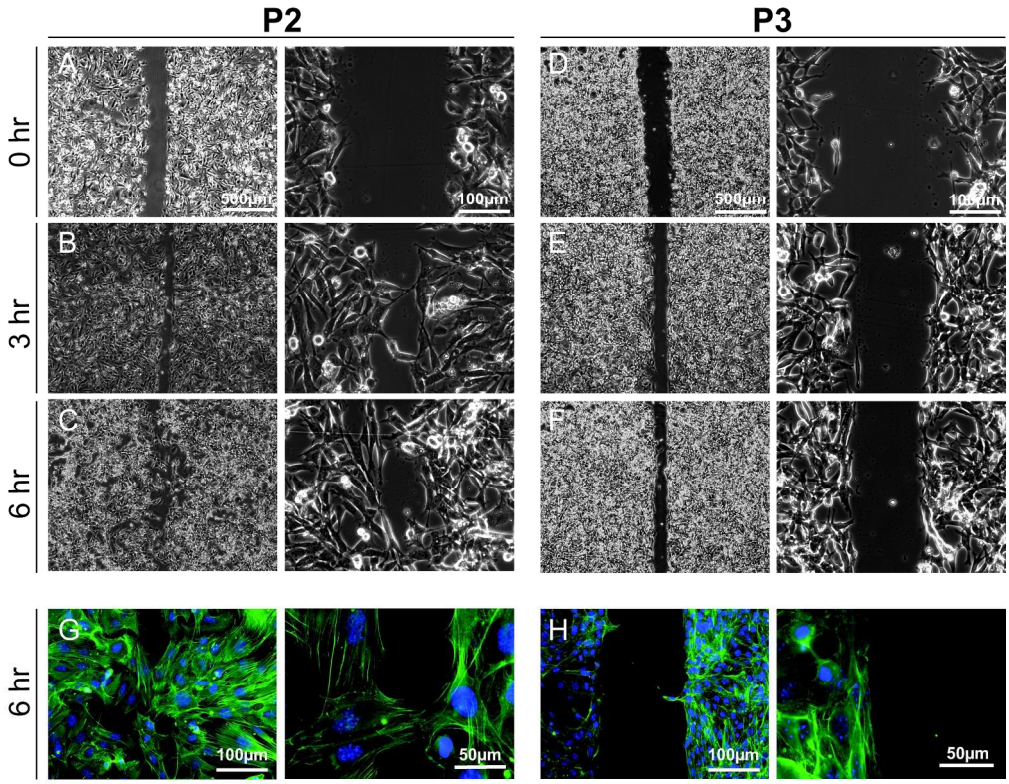

Figure 3.

Figure 3. Scratch test on Fn-coated glass slides. Lower (LEFT) and higher (RIGHT) magnification phase images were taken of P2 (A-C, G) and P3 (D-F, H) cultures immediately (A, D), 3 hr (B, E), and 6 hr (C, F, G, H) after creating a scratch of confluent monolayers. Samples fixed at 6 hr and stained with phalloidin were imaged fluorescently to visualize outstretched cellular processes.
222x193mm (300 x 300 DPI)

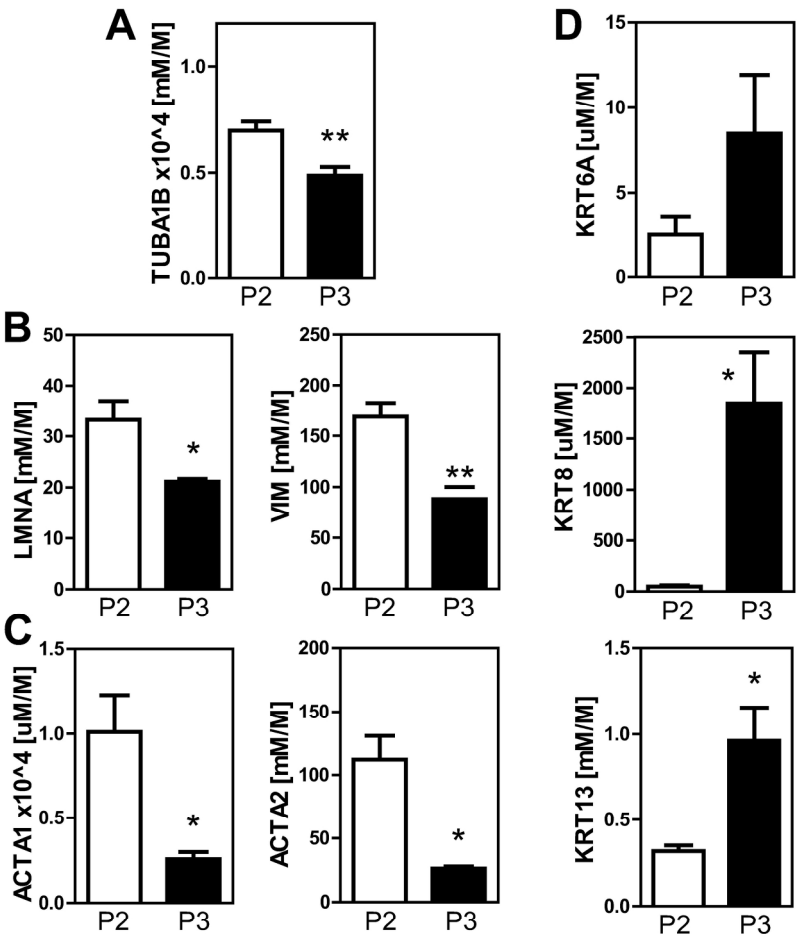

Figure 4.

Figure 4. Cytoskeletal gene expression on Fn-TCP. P2 and P3 cultures were analyzed for microtubules (A: TUBA1B), intermediate filaments (B: LMNA, VIM; D: KRT6A, KRT8, KRT13), and microfilaments (C: ACTA1, ACTA2). Values presented are mean±SEM (n=5), with asterisks indicating p-values (* for $p<0.05$, ** for $p<0.01$).
203x206mm (300 x 300 DPI)

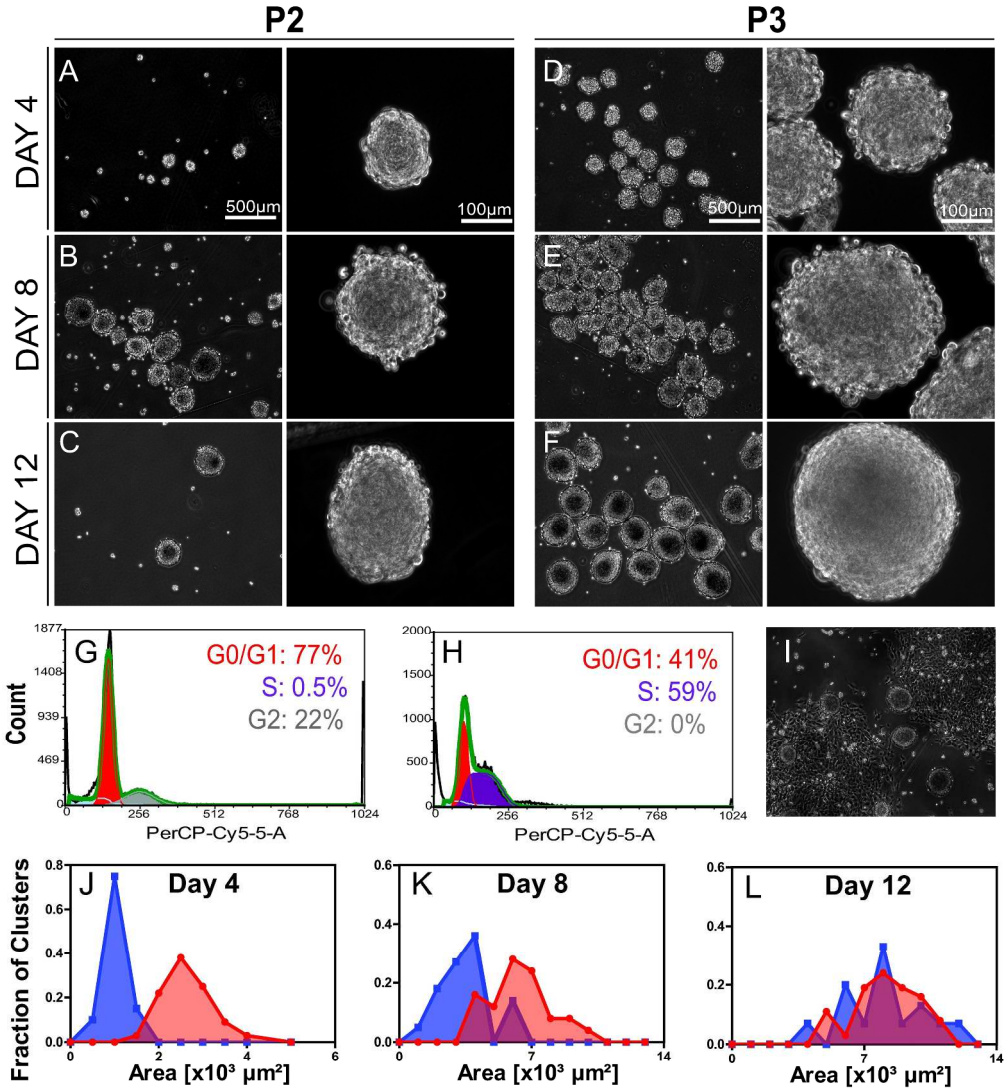

Figure 5.

Figure 5. Morphology and proliferation in SUS. Lower (LEFT) and higher (RIGHT) magnification phase images were taken of P2 (A-C) and P3 (D-F) cell clusters after 4 (A, D), 8 (B, E), and 12 (C, F) days. Histograms show fluorescence due to DRAQ5 staining for P2 (G) and P3 (H) SUS samples, with fitted curves for cell cycle overlayed to determine percentages in the G0/G1, S, and G2 phases (indicated by separate colors). (I) Phase image of P2 cells attached to petri dishes at Day 5. Histograms of size analysis for P2 (BLUE) and P3 (RED) cell clusters after 4 (J), 8 (K), and 12 (L) days.
276x323mm (300 x 300 DPI)

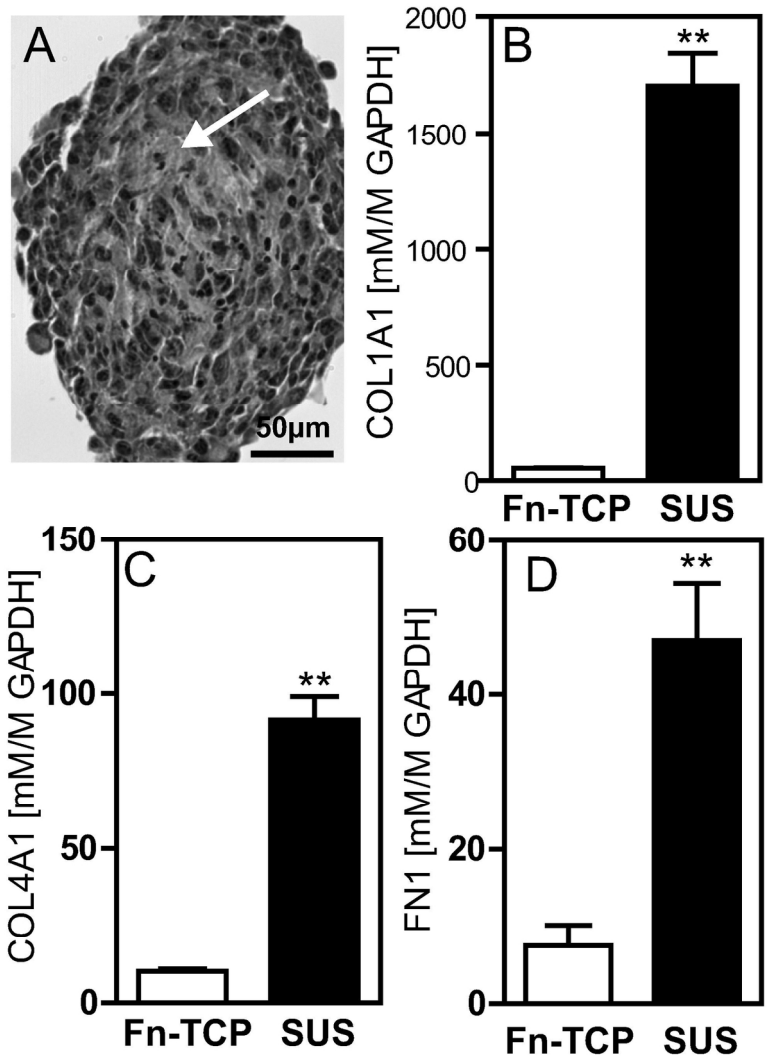

Figure 6.

Figure 6. Extracellular matrix of P3 cells in SUS. (A) Phase image of a D8 P3 cell cluster, arrow indicates granular matrix between cells. Relative gene expression of collagen type I (B), collagen type IV (C), and fibronectin (D) of P3 cells at D8 grown in SUS compared to Fn-TCP. Values presented are mean±SEM (n=3-5, ** for $p<0.01$).
131x206mm (300 x 300 DPI)

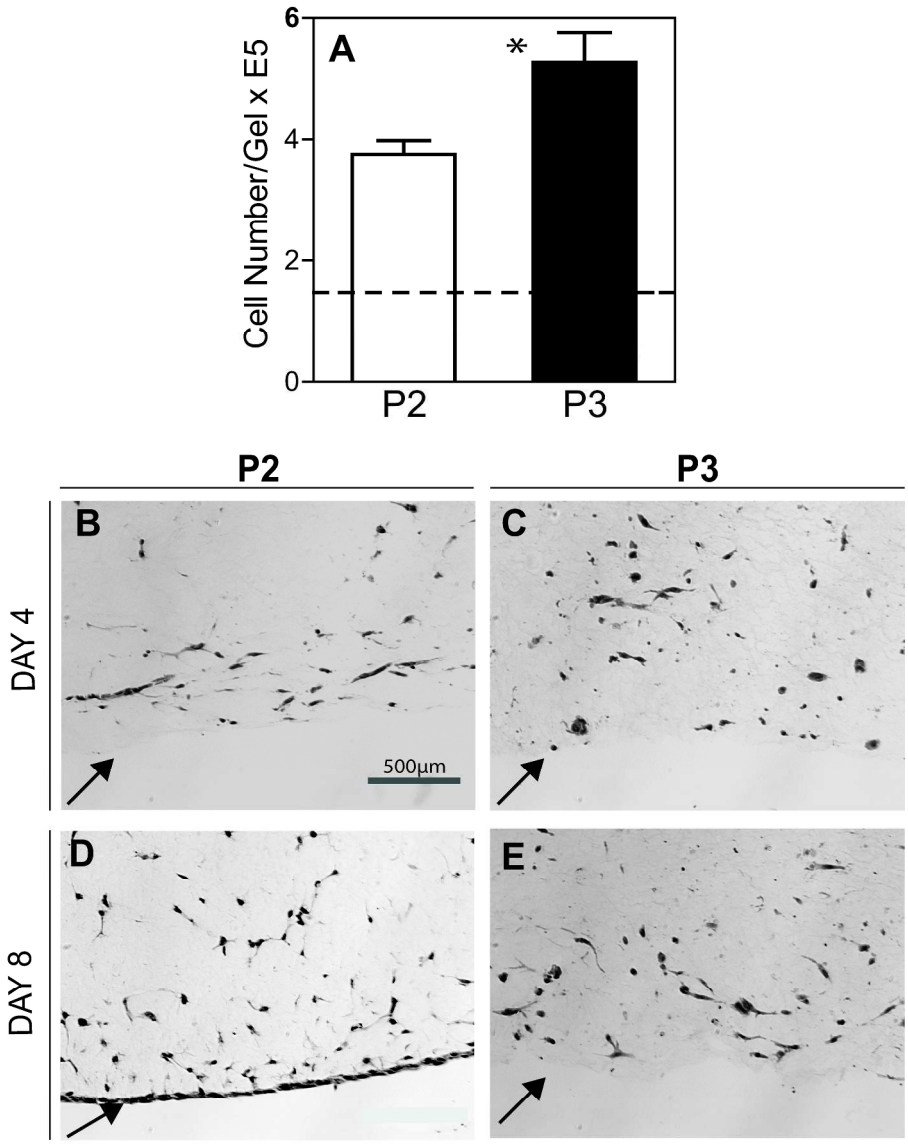

Figure 7.

Figure 7. Cell number and distribution in GEL samples. (A) Cell number was determined for P2 and P3 GEL samples after 4 days of culture, with the dotted line representing the initial cell number (mean±SEM, n=4, *for $p<0.05$). Brightfield images of P2 (B, D) and P3 (C, E) samples at 4 (B, C) and 8 (D, E) days are shown, with arrows indicating the edge of the collagen gels in cross-section.
273x363mm (300 x 300 DPI)

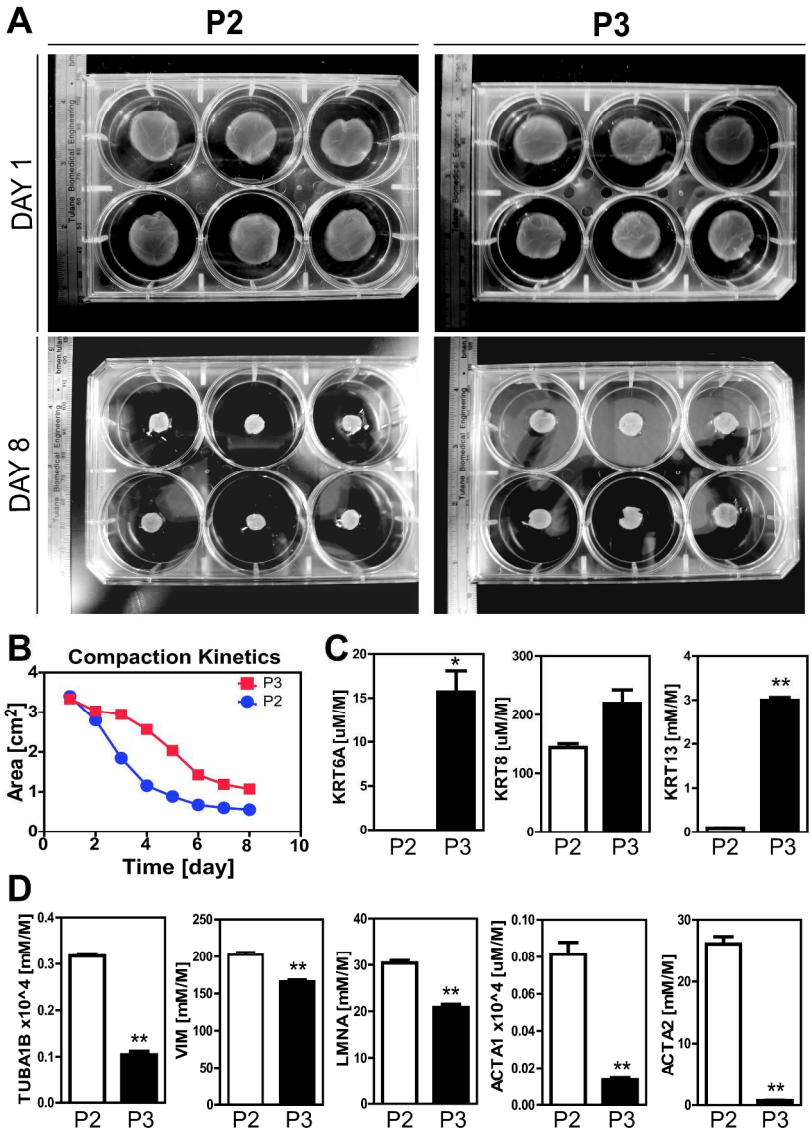

Figure 8.

Figure 8. Compaction and cytoskeletal expression in GEL samples. Macroscopic images are shown (A) for P2 (LEFT) and P3 (RIGHT) GEL samples at Days 1 and 8, with cross sectional area plotted for each day to quantitate compaction (B; mean±SEM, n=6-15). Cytoskeletal gene expression was analyzed in Day 8 samples for keratin filaments (C: KRT6A, KRT8, and KRT13), as well as other cytoskeletal proteins (D: TUBA1B, VIM, LMNA, ACTA1, and ACTA2). Values presented are mean±SEM (n=3), with asterisks indicating p-values (* for $p<0.05$, ** for $p<0.01$).
281x416mm (300 x 300 DPI)

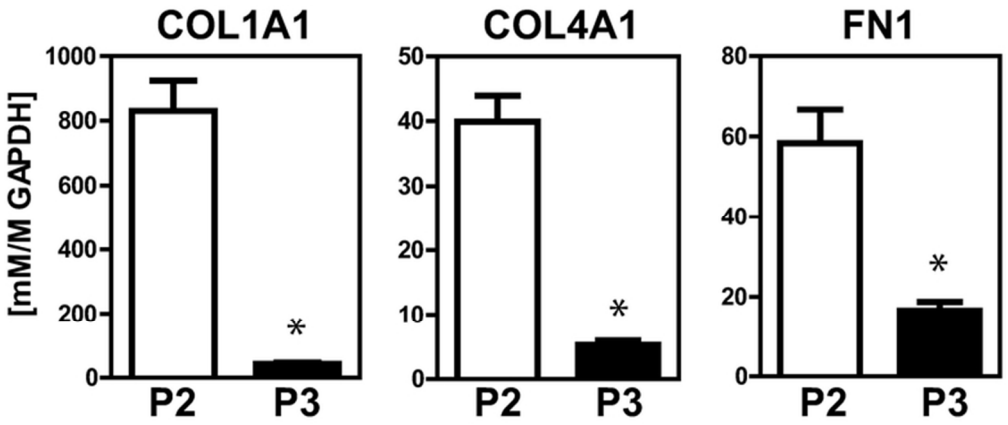

Figure 9.

Figure 9. Extracellular matrix in GEL samples. P2 and P3 GEL samples at Day 8 were analyzed for relative gene expression of collagen type I, collagen type IV, and fibronectin. Values presented are mean±SEM (n=3, * for $p<0.05$).
65x34mm (300 x 300 DPI)

Symbol	Gene Name	Forward Sequence (5' to 3')	Reverse Sequence (5' to 3')	Genebank Accession Number
ACTA1	Actin, alpha 1, skeletal muscle	CACCCAGGGCCAGAGTCA	GCGATGTGAGTGATCTGCTGTAGG	NM_009606
ACTA2	Actin, alpha 2, smooth muscle	TCCCTGGAGAAGAGCTACGAACT	AAGCGTTCGTTTCCAATGGT	NM_007392
TUBA1B	Tubulin, alpha 1B	CGCCTTCTAACCCGTTGCT	TGGCCAACGTGGATGGA	NM_011654
KRT6A	Keratin 6A	TGCCCTGCCGTTTCTCTACT	TGGTTTTGGTAGACATGGTTCCT	NM_008476
KRT8	Keratin 8	TGGTGTCCGAGTCTTCTGATGT	CAGGCTGGCAAGGACTTCA	NM_031170
KRT13	Keratin 13	TCCAACGCTGAAATGATCCA	GGAGTGTGCGCCTGAGTTCT	NM_010662
LMNA	Lamin A	CGCAGCATGCTCGCACTA	ACGAACTTTCCCTCTTCATCGA	NM_001002011
VIM	Vimentin	GAGAGAGGAAGCCGAAAGCA	GCCAGAGAAGCATTGTCAACATC	NM_011701
Col Ia1	Collagen Type I, Alpha 1	CTTCACCTACAGCACCCTTGTG	TGACTGTCTTGCCCCAAGTTC	NM_007742.3
Col4a1	Collagen Type IV, Alpha 1	CCTGGCGCTTCTTGCTTCT	AGTCTGTGGTTAGTGTTGCAAACC	NM_009931.1
FN1	Fibronectin 1	GTGTAGCACAACTTCCAATTACGAA	GGAATTTCCGCCTCGAGTCT	NM_010233.1
GAPDH	Glyceraldehyde-3-phosphate dehydrogenase	GCCTTCCGTGTTCCTACC	GCCTGCTTCACCACCTTC	NM_008084

Supplemenal Table 1. List of PCR primers used to amplify genes for cytoskeleteal and extracellular matrix proteins.

		P2 Fn-TCP/P3 Fn-TCP		P2 SUS/P3 SUS		P2 SUS/P2 Fn-TCP		P3 SUS/P3 Fn-TCP	
Symbol	Description	Fold Reg	P-value	Fold Reg	P-value	Fold Reg	P-value	Fold Reg	P-value
Atf2	Activating transcription factor 2	-1.31	0.05	-1.14	0.18	1.80	0.01	1.57	0.00
Bax	Bcl2-associated X protein	-1.36	0.09	-1.20	0.05	1.01	1.00	-1.13	0.34
Bcl2	B-cell leukemia/lymphoma 2	1.22	0.04	1.31	0.08	1.01	0.91	-1.07	0.34
Bcl2l1	Bcl2-like 1	-1.74	0.01	1.35	0.04	-1.01	0.96	-2.36	0.00
Birc2	Baculoviral IAP repeat-containing 2	-1.19	0.33	-1.28	0.15	1.49	0.05	1.59	0.04
Birc3	Baculoviral IAP repeat-containing 3	1.12	0.58	-1.52	0.01	5.59	0.00	9.53	0.00
Birc5	Baculoviral IAP repeat-containing 5	-1.42	0.04	1.02	0.62	-1.17	0.03	-1.69	0.01
Bmp2	Bone morphogenetic protein 2	-49.93	0.01	-12.12	0.00	127.82	0.00	31.02	0.00
Bmp4	Bone morphogenetic protein 4	1.13	0.17	-1.08	0.71	1.22	0.25	1.48	0.00
Brca1	Breast cancer 1	-1.24	0.01	-1.15	0.14	1.01	0.81	-1.06	0.43
Ccl2	Chemokine (C-C motif) ligand 2	3.83	0.03	1.16	0.08	11.73	0.00	38.78	0.00
Ccl20	Chemokine (C-C motif) ligand 20	-2.68	0.00	-5.02	0.04	10.78	0.00	20.20	0.02
Ccnd1	Cyclin D1	-2.04	0.00	1.01	0.96	-1.74	0.00	-3.60	0.00
Cd5	CD5 antigen	1.49	0.22	1.03	0.94	1.56	0.25	2.25	0.04
Cdh1	Cadherin 1	-1.44	0.31	1.32	0.15	1.39	0.24	-1.37	0.28
Cdk2	Cyclin-dependent kinase 2	1.28	0.02	1.04	0.67	1.18	0.07	1.46	0.01
Cdkn1a	Cyclin-dependent kinase inhibitor 1A (P21)	1.24	0.32	-1.51	0.04	1.79	0.02	3.36	0.00
Cdkn1b	Cyclin-dependent kinase inhibitor 1B	-1.23	0.11	-1.33	0.07	-1.38	0.03	-1.27	0.10
Cdkn2a	Cyclin-dependent kinase inhibitor 2A	464.73	0.00	362.03	0.00	-1.08	0.50	1.18	0.03
Cdkn2b	Cyclin-dependent kinase inhibitor 2B (p15, inhibits CDK4)	11236.82	0.00	7496.54	0.00	-1.14	0.13	1.32	0.31
Cebpb	CCAAT/enhancer binding protein (C/EBP), beta	-1.33	0.31	1.19	0.07	2.76	0.00	1.75	0.06
Csf2	Colony stimulating factor 2 (granulocyte-macrophage)	-1.95	0.11	4.35	0.05	3.81	0.04	-2.22	0.16
Cxcl1	Chemokine (C-X-C motif) ligand 1	4.37	0.08	-1.05	0.80	1.18	0.76	5.44	0.01
Cxcl9	Chemokine (C-X-C motif) ligand 9	-1.48	0.21	-1.34	0.33	5.53	0.00	5.01	0.03
Cyp19a1	Cytochrome P450, family 19, subfamily a, polypeptide 1	-3.04	0.04	-1.43	0.05	19.01	0.00	8.96	0.00
Egr1	Early growth response 1	-1.02	0.78	-1.39	0.10	1.12	0.28	1.52	0.21
Ei24	Etoposide induced 2.4 mRNA	-1.43	0.05	-1.48	0.00	1.42	0.02	1.47	0.01
En1	Engrailed 1	18.95	0.00	16.06	0.00	-1.05	0.85	1.13	0.39
Fas	Fas (TNF receptor superfamily member 6)	2.29	0.02	-2.23	0.00	1.01	0.99	5.14	0.00
Fasl	Fas ligand (TNF superfamily, member 6)	1.93	0.95	-1.14	0.50	1.07	0.60	2.35	0.50
Fasn	Fatty acid synthase	-1.27	0.20	-1.15	0.25	1.50	0.02	1.36	0.11
Fgf4	Fibroblast growth factor 4	2.21	0.12	2.25	0.20	1.49	0.43	1.46	0.26
Fn1	Fibronectin 1	1.65	0.10	-1.14	0.55	2.02	0.02	3.80	0.02
Fos	FBJ osteosarcoma oncogene	2.26	0.53	1.10	0.70	1.67	0.96	3.44	0.26
Foxa2	Forkhead box A2	-3.00	0.00	-1.40	0.32	2.10	0.08	-1.02	0.92
Gadd45a	Growth arrest and DNA-damage-inducible 45 alpha	-2.48	0.30	1.35	0.15	1.97	0.00	-1.71	0.39
Greb1	Gene regulated by estrogen in breast cancer protein	-1.41	0.15	1.71	0.00	3.13	0.00	1.30	0.08
Gys1	Glycogen synthase 1, muscle	-1.55	0.13	-1.43	0.02	-1.15	0.16	-1.24	0.34
Hhip	Hedgehog-interacting protein	-1.98	0.02	1.05	0.65	1.53	0.09	-1.37	0.07
Hk2	Hexokinase 2	-2.11	0.02	-1.75	0.01	-1.76	0.00	-2.11	0.02
Hoxa1	Homeo box A1	1.34	0.06	-1.49	0.05	-2.55	0.00	-1.27	0.06
Hsf1	Heat shock factor 1	-1.59	0.02	-1.00	0.98	1.66	0.06	1.04	0.75
Hspb1	Heat shock protein 1	4.33	0.02	1.09	0.53	2.89	0.00	11.46	0.00
Icam1	Intercellular adhesion molecule 1	-2.40	0.03	1.31	0.09	37.44	0.00	11.92	0.00
Igfbp3	Insulin-like growth factor binding protein 3	-384.43	0.00	-4.65	0.00	112.34	0.01	1.36	0.04
Igfbp4	Insulin-like growth factor binding protein 4	-18.97	0.02	1.04	0.66	31.79	0.00	1.61	0.09
Ikbkb	Inhibitor of kappaB kinase beta	-1.40	0.11	-1.14	0.19	1.41	0.08	1.16	0.24
Il1a	Interleukin 1 alpha	-1.66	0.15	3.72	0.00	5.89	0.00	-1.05	0.82
Il2	Interleukin 2	-1.25	0.30	1.10	0.75	1.92	0.05	1.39	0.20
Il2ra	Interleukin 2 receptor, alpha chain	2.78	0.38	-1.05	0.87	-1.85	0.39	1.57	0.03
Il4ra	Interleukin 4 receptor, alpha	1.56	0.02	1.19	0.05	2.33	0.00	3.03	0.00
Irf1	Interferon regulatory factor 1	-1.02	0.84	-1.45	0.02	2.36	0.01	3.36	0.00
Jun	Jun oncogene	-1.61	0.17	-1.00	0.91	-1.08	0.62	-1.73	0.11
Lef1	Lymphoid enhancer binding factor 1	1.20	0.15	10.59	0.00	7.38	0.00	-1.19	0.50
Lep	Leptin	-1.28	0.26	-1.07	0.81	1.79	0.08	1.50	0.01
Lta	Lymphotoxin A	-1.37	0.20	1.11	0.60	1.50	0.22	-1.02	0.84
Mdm2	Transformed mouse 3T3 cell double minute 2	-1.32	0.09	-1.02	0.83	1.40	0.01	1.08	0.65
Mmp10	Matrix metallopeptidase 10	-1.46	0.09	-1.02	0.67	2381.79	0.00	1668.44	0.00
Mmp7	Matrix metallopeptidase 7	-1.83	0.14	-1.25	0.32	2.56	0.01	1.75	0.11
Myc	Myelocytomatosis oncogene	-2.22	0.03	-3.43	0.01	-2.12	0.00	-1.37	0.28
Nab2	Ngfi-A binding protein 2	-1.56	0.15	-1.03	0.93	-1.05	0.87	-1.59	0.15
Naip1	NLR family, apoptosis inhibitory protein 1	2.41	0.22	3.80	0.01	25.87	0.00	16.43	0.00
Nfkbia	Nuclear factor of kappa light polypeptide gene enhancer in B-cells inhibitor, alpha	1.54	0.07	-1.29	0.08	3.12	0.00	6.21	0.00
Nos2	Nitric oxide synthase 2, inducible	-2.01	0.05	-1.56	0.06	1.51	0.21	1.17	0.42
Nrip1	Nuclear receptor interacting protein 1	-1.92	0.02	-1.06	0.65	1.62	0.01	-1.12	0.49
Odc1	Ornithine decarboxylase, structural 1	-2.86	0.01	1.27	0.00	1.24	0.01	-2.95	0.01
Pmepa1	Prostate transmembrane protein, androgen induced 1	2.21	0.00	2.27	0.01	4.30	0.00	4.19	0.00
Pparg	Peroxisome proliferator activated receptor gamma	-1.06	0.68	1.76	0.01	-1.97	0.00	-3.69	0.04
Ptch1	Patched homolog 1	1.00	0.97	-1.22	0.16	1.13	0.41	1.39	0.05
Ptgs2	Prostaglandin-endoperoxide synthase 2	-1.77	0.19	-1.09	0.53	1.87	0.04	1.15	0.77
Rbp1	Retinol binding protein 1, cellular	1.12	0.71	2.27	0.02	24.33	0.00	12.01	0.02
Sele	Selectin, endothelial cell	-1.15	0.70	33.69	0.00	66.94	0.00	1.72	0.01
Selp	Selectin, platelet	4.91	0.04	17.88	0.00	7.24	0.00	1.99	0.05
Tank	TRAF family member-associated Nf-kappa B activator	1.33	0.02	1.12	0.19	1.41	0.00	1.67	0.01
Tcf7	Transcription factor 7, T-cell specific	-1.80	0.02	-1.42	0.02	17.92	0.00	14.11	0.00
Tert	Telomerase reverse transcriptase	-1.67	0.00	1.67	0.02	2.04	0.01	-1.36	0.00
Tfrc	Transferrin receptor	-1.87	0.12	1.54	0.01	-1.52	0.04	-4.40	0.03
Tnf	Tumor necrosis factor	1.69	0.37	1.93	0.56	4.47	0.07	3.91	0.18
Trp53	Transformation related protein 53	-1.56	0.00	-1.13	0.20	1.55	0.00	1.13	0.22
Vcam1	Vascular cell adhesion molecule 1	2.12	0.00	-1.39	0.00	6.00	0.00	17.66	0.00
Vegfa	Vascular endothelial growth factor A	-1.47	0.32	1.50	0.06	1.35	0.07	-1.64	0.26
Wisp1	WNT1 inducible signaling pathway protein 1	4.87	0.00	-1.57	0.01	1.20	0.08	9.16	0.00
Wnt1	Wingless-related MMTV integration site 1	-1.44	0.06	-1.02	0.96	1.93	0.05	1.37	0.15
Wnt2	Wingless-related MMTV integration site 2	4.29	0.17	1.94	0.63	1.37	0.80	3.04	0.29
	HOUSEKEEPING GENES & INTERNAL CONTROLS								
Gusb	Glucuronidase, beta								
Hprt1	Hypoxanthine guanine phosphoribosyl transferase 1								
Hsp90ab1	Heat shock protein 90 alpha (cytosolic), class B member 1								
Gapdh	Glyceraldehyde-3-phosphate dehydrogenase								
Actb	Actin, beta								
MGDC	Mouse Genomic DNA Contamination								
RTC	Reverse Transcription Control								
RTC	Reverse Transcription Control								
RTC	Reverse Transcription Control								
PPC	Positive PCR Control								
PPC	Positive PCR Control								
PPC	Positive PCR Control								

Supplemental Table 2. Gene Expression of signaling pathways. List of 84 signaling-related genes and the respective fold-regulation for groups: P2 Fn-TCP/P3 Fn-TCP, P2 SUS/P3 SUS, P2 SUS/P2 Fn-TCP and P3 SUS/P3 Fn-TCP.